ADVANCED ELECTROMAGNETICS, VOL. 6, NO. 2, MARCH 2017

Nano Energy Harvesting with Plasmonic Nano-Antennas:

A review of MID-IR Rectenna and Application

Rocco Citroni[1], Alberto Leggieri[1], Davide Passi[1], Franco Di Paolo[1], Aldo Di Carlo[1]

[1]Department of Electronic Engineering, University of Rome Tor Vergata, Italy

*corresponding author, Email: (rocco.citroni@uniroma2.it)

Abstract

Drones, a technical nickname for unmanned aerial vehicles (UAVs) are gaining more and more interest and popularity. Supported by the miniaturization and cost reduction of electronic components, a new class of UAVs called Nano-air vehicles or NAVs represent the future technology for indoor and outdoor mission. One of the main considerations when building or buying a drone is the flight time and range. The flight time is nowadays a drawback for miniature unmanned aerial vehicles (UAVs). It is limited to a few minutes before requiring a forced recovery to replace exhausted batteries. Currently the batteries are the dominant technology, which possess limited operation in time and energy. The real viability to extending flight time (FT) of NAVs is possibly exploring new and more disruptive alternative solution able either to recharge a battery, or even to directly power the NAVs during the flight. A Plasmonic Nano Energy harvester is an attractive technology to extending the FT extracting the energy in mid-infrared radiation emitted from Earth's surface with Rectenna tuned to mid-infrared wavelengths $(7 - 14\mu m)$ with a peak wavelength of about 10μm . In this review the concepts emerging from this work identify and suggest how this novel harvester can constantly supply these flying objects for the whole day.

Keywords—NAV; Nano Energy Harvesting; Plasmonic Harvester; MIM-MIIM

1. Introduction

Designed to provide short range "over-the-hill", or "around-the corner" information, today the task of unmanned air vehicles (UAVs) is to support reconnaissance, surveillance, and target acquisition (RSTA) mission. Thanks to miniaturization and ultralow power technique, a new class of unmanned named NAVs (Nano Air Vehicles) is emerging. The class of NAVs is lightweight, man-portable and hand launch-able. Nano-drones are minuscule Nano flight robots split into two sub-sections: autonomous aircraft and remotely piloted aircraft. They are capable of transferring data, such as live footage, back to base, designed for quick assembly and disassembly during field deployment [1]. Figure 1 shows an example of black UAV Hornet Nano helicopter.

Figure 1: Black UAV Hornet Nano helicopter "photo on courtesy by Proxdynamics"[3]

Designed for short range utility, the unit measures about 10 (length) ×2.5(width) cm, has maximum flight altitude around 100 m, with a 10m/s maximum speed and maximum takeoff weight (MTOW= Mass + Payload) of 20 g (battery included). The maximum flight time is approximately 20 minutes, powered by high energy density lithium-ion or lithium polymer batteries [2]. The Nano-robot can be operated almost anywhere at any time without prior airspace coordination. The small size and electric motors makes it virtually inaudible and invisible beyond short distances particularly at night. Nevertheless, one of the main drawbacks faced today is the flight time, directly limited by the on-board battery capacity [4]. The other key drawbacks are the weight and size of the NAV, which restrict the mounting of larger payloads or extra batteries. The design challenge is to generate and store enough energy to maximize flight time. Currently for unmanned systems, batteries represent the dominant technologies. They represent a significant fraction of the total size and weight of the system. The battery's energy density (energy per mass) is the essential parameter in this context. A higher energy density enables longer flight times and lighter aircraft [5]. However, the batteries are not very efficient in particular mission where recharging them is impossible for example in toxic and radiation

environments. We accept their limitations (such as short lifetime, long recharge time, etc.) simply because there are no real alternatives [4]. Currently when the battery is running low, we need to force some robots to return to change their batteries. One possibility to overcome these power limitations is to extract (harvest) energy from the environment. These forms of energy will allow creating a highly efficient and self-powered system able to provide unlimited energy supply to NAVs. This is a newly emerging field of *Nano-energy* [6]. Although particular harvester as photovoltaics (PV) technologies has improved the flight time, PV is not an "always-on" power source, in fact it is limited in two major ways: by the availability of light and the absorbed wavelengths [7,8]. A new idea is proposed. As with any object in thermal equilibrium, Earth absorbs solar energy from the sun during daytime and then continuously re-emits it at day and night. At thermal equilibrium, the Earth absorbs and re-emits the same amount of energy. The peak wavelength of this re-radiation spectrum falls at around 10 µm [9, 10]. So if an antenna could detect this wavelength, it could also convert it into electricity. Assuming the antenna is not in thermal equilibrium with its surroundings it is possible to scavenge energy from the environment without violating the second law of thermodynamics [11]. Rectennas (Nano antennas coupled to a tunneling diode) that use excited localized surface plasmons tuned to the Mid-IR can harvest IR energy from the sun at night and day and convert it into DC electricity to energize Nano-drones all day. The principal advantage of the proposed technique is that it employs plasmonic Rectennas that absorb the incident IR radiation treating it as electromagnetic waves inducing a AC current in the antenna surface. The antennas rely on natural resonance [12]. Subsequently the AC current will be rectified to energize the load. The paper is organized as follows: Section 2 presents the equations to estimate flight time and range for NAVs. Section 3 presents a circuit model of the IR antenna coupled to rectifying diode. A review of wideband Nano Antennas tuned to the Mid-IR that uses excited localized surface plasmons, is reported in subsection of Section 3. Section 4 shows the status of rectifiers, the challenge in Mid-IR range and the proposed solution. Finally, Section 5 provides concluding remarks.

1.1 Possible Area of Applications

In today's world, civil security is of major importance. In protecting the public from threats such as terrorist attacks and in successfully identifying crimes, appropriate air support can be a decisive advantage. Helicopters can be an important source of support to teams on the ground. However, as a form of air support they are expensive and can take time to be ready for engagement. The UAV are less expansive, in particular Nano-drones have a quick assembly and disassembly during field deployment. A Nano-drone can be instantly ready for action, allowing for immediate air support. In disaster monitoring inside tunnels or buildings while large UAV cannot be deployment, a Nano-drone can act immediately, without any loss of time. In several scenarios, where the human intervention is not possible, e.g., in toxic and radiation small area using NAVs can provide a useful support. It is important to be able to obtain a rapid overview of the situation that is often only possible from the sky. In the future, using the optional waypoint navigation function will allow to Nano-drones to inspect the relevant installation autonomously, without the need for navigation instructions from a pilot [13, 14, 15, 16].

2.0 Equations to Estimate Flight Time and Range of NAV

One of the main considerations when building or buying a drone is the flight time and range. Batteries currently power all components on board NAV as electronic circuits, sensors, actuators, and the communication devices. Factors as capacity and energy density of battery allows longer flight time. However, to increase the flight time is necessary to increase the capacity with resulting in increased battery size. Many factors affect the correct calculation of the flight time as hovering or sportive flying, cable, turbulence, battery type. [17, 18, 19]. The table 1 shows the materials list of a commercial NAV and their weight budget.

Table 1: materials list of NAV and their weight budget.

NAV Helicopter Components	Weight (g)
Flight Control Board	3
Battery	1.5
Camera Board	1
Antenna	2
Motor /propellers	4.9/2.5
TX/RX	2
Speed Controller	0.70
Actuator	3
Cables	1
Frame	2
Total Weight	21

To estimate the flight time the author considers two flight conditions, full throttle and hovering. The force generated by the rotor must be more than the weight (at least 2:1) of the NAV otherwise, would not be able to take off vertically. Smaller UAVs (usually the size of the palm of your hand) tend to use small-brushed

motors. Let's assume a helicopter's weight (including frame, motors, electronics, battery, accessories etc.) to be 20g. Each motor should therefore be capable of providing (20g/1 motor) x 2:1 = 40g of thrust (or more). The figure 2 shows the required current that the motor needs to Full Throttle:

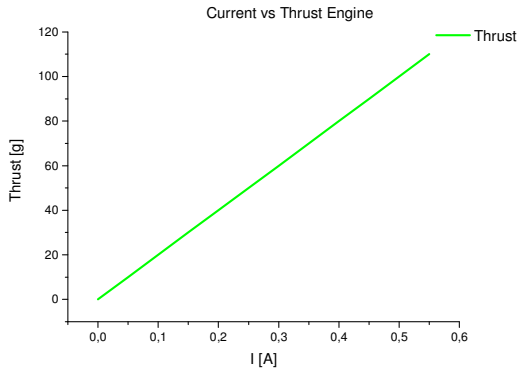

Figure 2: Curve shows the correlation between engine thrust and current battery

Assume user is using 75% throttle of the time to fly around, and the rest of the time hovering, the current draw in throttle for 40 g of thrust will be 0.20 A, in the hovering time the current will be supposed 10 % less (This is purely estimation). What will be the maximum flight time and range assuming a single battery on board Nano robot with a minimum capacity of 90 mAh? [17,18,19]. To calculate the flight time in both flight condition we should consider the following losses (wind, hovering or sportive flying, cable, turbulence...) for this reasons we estimate ~10% losses [20].

$t_{Throttle} = 0.90 \cdot 60 \cdot (\frac{\frac{C}{1000} \cdot N_{batt}}{I_{tot}})$ Full throttle flight time based on the battery capacity and motor current with margin of error due to the exclusion of electronics, accessories (1)

$t_{Hover} = 0.90 \cdot 60 \cdot (\frac{\frac{C}{1000} \cdot N_{batt}}{I_{Htot}})$ Hover flight time based on the battery capacity and motor current with margin of error due to the exclusion of electronics, accessories (2)

$t_{average} = (\frac{t_{hover} + t_{throttle}}{2})$ Average flight time (3)

Where:

C is the capacity of battery = 90 mAh

N_{batt} is the number of battery on board NAV = 1

$I_{tot} = I_{motor} \cdot N_{motor}$ Total Full throttle UAV current (4)

$I_{Htot} = I_{Hmotor} \cdot N_{motor}$ Total hover UAV current (5)

N_{motor} is the number of motor on board NAV=1

The results for Throttle and hover condition are presented in table 2 and table 3below.

Table 2: Results for NAV in Throttle condition

Throttle	Equation	Results	Unit
Thrust	/	40	g
I_{mot}	Figure 2	0.20	A
I_{tot}	4	0.20	A
$t_{Throttle}$	1	24.3	min
Range	7	2.035x10^3	m
$t_{average}$	3	25.65	min

Table 3: Results for NAV in Hover condition

Hover	Equation	Results	Unit
Thrust	/	40	g
I_{Hmot}	Figure 2	0.18	A
I_{Htot}	5	0.18	A
t_{Hover}	2	27	min
Range	7	/	m
$t_{average}$	3	25.65	min

The simulation in figure 3 shows the results of flight time vs battery capacity respectively in throttle and hover condition

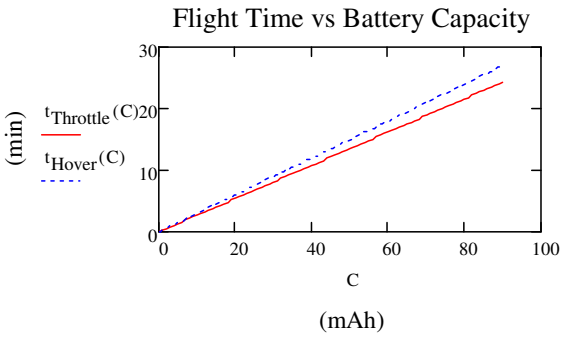

Figure 3: Flight time in Throttle and Hover condition vs Battery Capacity

The figure 3 shows that the flight time in both conditions increases as a function of the battery capacity. However, as the capacity of battery gets larger, the increase in flight time becomes ineffective. In fact there will be a point where it just does not gain any more flight time with bigger battery (even lose flight time). The figure 3 shows that the advantage in hover condition is only of three minutes on throttle condition.

2.1 Range of NAV

The equation 7 shows, known the motor efficiency and specific energy of the battery, how the payload's weight could affect the range of a UAV. D'Angelo estimates the energy requirement to be [21]:

$$\frac{d}{1-v_r}\left(\frac{m_p+m_v}{370\eta r}+\frac{p}{v_c}\right) \qquad (6)$$

The range d in km is:

$$d=\frac{2\cdot E_b(1-v_r)}{\left(\frac{m_p+m_v}{370\eta r}+\frac{p}{v_c}\right)} \qquad (7)$$

Where E_b is the source specific energy of the battery (for Li-Po 100-265 Wh/Kg), m_p = payload mass in g, m_v = vehicle mass in g, r = lift-to-drag ratio, η = power transfer efficiency for motor and propeller, p = power consumption of electronics in W, v_r = ratio of headwind to airspeed and v_c = cruising velocity of the aircraft in m/sec. We assume η to be 0.5, and r to be 3. It is clear that advances in battery source specific energy will drastically increase flight time and range. The table 4 shows the values used in (7) to calculate the maximum range of NAV.

Table 4: Summaries of values used in (7) to calculate the maximum range of NAV.

E_b (Wh/kg)	V_r	m_p (g)	m_v (g)	η	r	p (W)	V_c (m/sec)
(100-265)	0.3	1	19	0.5	3	0.74	5

The Figure 4 shows the range as a function of payload mass. The aircraft's range is roughly proportional to the payload mass. As payload mass is increased, the total weight of the aircraft increases. Increasing the weight raises the minimum speed of the aircraft and reduces the throttle range.

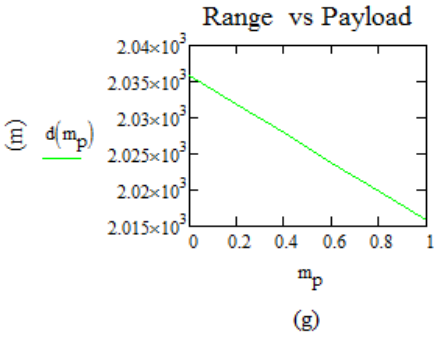

Figure 4: Range NAV vs Payload mass

The Figure 5 plots the range as a function of cruising velocity and motor efficiency. The variation of motor efficiency with cruising velocity leads to increase the range. This will involve the power will have increase because the motor will have to spin faster, and thus pull more current.

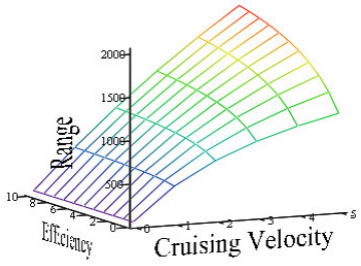

Figure 5: Range of NAV as a function of motor efficiency and cruising velocity

3.0 Energy Harvesting Principles

Figure 6 shows the block diagram of a self-powered system that harvests energy from the environment. The classic (high-efficiency) energy-harvester system consists of an energy generator, capture/storage/management electronics and a load designed to be powered by the harvester. The first block of diagram below, the transducer is a plasmonic harvester. It is shown as the energy generator. The plasmonic generator transforms IR electromagnetic wave, into electrical voltage/current. The energy-conditioning block is used to properly charge the storage unit. The power-conditioning block provides the appropriate power supply to the load. A second key component of energy management is storage and retention, with minimal leakage or loss. When the source is minimum, there may be extended time intervals before sufficient energy has been captured and stored. Therefore, the harvester's electronic design must possess extremely high retention when the energy-generator function is randomly available or interrupted for long periods of time [22,23].

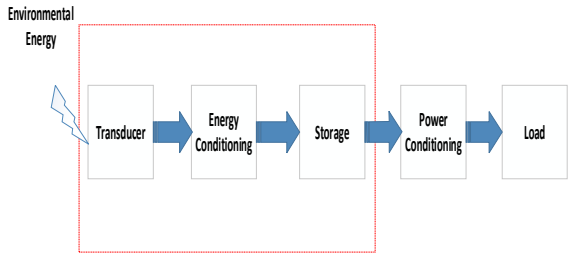

Figure 6: Block diagram of a self-powered system. The blocks inside the dashed red box form the energy harvester subsystem.

The capturing, accumulating and storing of small packets of electrical energy requires high efficiency. The circuit must stay in the active mode and be ready to perform the capture whenever harvestable energy becomes available. The device must be ready to provide an output as the application design requires it. The efficiency must be high enough so that the energy consumed by the load is much smaller than the energy provided by the generating source. At any instant of time t the amount of energy consumed at node i (NAV) is [24]:

$$E(i,t) = \int_{t_0}^{t} [P_s(i,t) - P_c(i,t)]dt \qquad (8)$$

Where $P_s(i,t)$ and $P_c(i,t)$ represents respectively the power of energy harvester and energy being consumed at that time t from node i. Therefore, a node is self-contained if:

$$E(i,t) > 0 \quad \forall t > 0 \qquad (9)$$

In fact, by formula 8 any energy received when $P_s(i,t) < P_c(i,t)$ is wasted. Also, when $P_s(i,t) \geq P_c(i,t)$, the energy $P_s(i,t) - P_c(i,t)$ is wasted. Due to the variability of environmental energy sources, a storage unit (battery or an ultra-capacitor) is needed to provide a constant power flow to the load. However, an energy storage mechanism is not ideal and present any criticality: the energy capacity is limited, the charging efficiency η is strictly less than 1 and some energy is lost through leakage. The conditions of energy conservation and buffer size limit are discussed below. First define a rectifier function $[x]^+$ as follows [25]:

$$[x]^+ = \begin{cases} x\_x \geq 0 \\ 0\_x < 0 \end{cases}$$

Energy conservation leads to:

$$B_0 + \eta\int_0^T [P_s(i,t) - P_c(i,t)]^+ dt - \int_0^T [P_c(i,t) - P_s(i,t)]^+ dt - \int_0^T P_{leak}(t)dt \geq 0$$
$$\forall T \in [0,\infty) \qquad (10)$$

Where, B_0 is the initial energy stored in the ideal energy buffer and $P_{leak}(i,t)$ is the leakage power for the energy buffer. The buffer size limit requires the following additional constraint to be satisfied:

$$B_0 + \eta\int_0^T [P_s(i,t) - P_c(i,t)]^+ dt - \int_0^T [P_c(i,t) - P_s(i,t)]^+ dt - \int_0^T P_{leak}(i,t)dt \leq B$$
$$\forall T \in [0,\infty) \qquad (11)$$

B is the size of the energy buffer.

The eq. (10) is a sufficient and necessary condition to be satisfied by all allowable $P_s(i,t)$ and $P_c(i,t)$ instead the condition (11) is only sufficient but not necessary. This happens because excess energy not used or stored in the buffer can be dissipated as heat from the system. In this case, the left-hand side of Eq. (10) will be strictly greater than zero, by the amount of energy wasted. The condition (11) becomes necessary if wasting energy is not allowed.

3.1 Proposed Novel Energy Harvester

Currently, the batteries represents the only dominant technology to energize the NAVs. However, batteries present several disadvantages: the need to replace or recharge them periodically and their big size and weight. To maximize the flying time weight and power budget should be carefully monitored. One possibility to overcome these power limitations is to extract (harvest) energy from the environment. These technologies can be

used to possibly replace or at least extend the lifetime of a battery. By using the energy from environment, our goal is therefore to make the system self-powered and energy independent. The idea therefore is to add an energy scavenging unit on board which would provide an unlimited source of power over the NAVs' lifetime. The mission period would no longer be limited by the power source, and no additional maintenance would be required for recharging or replacing the battery. To maximize the flying time, is of primary importance to investigate which harvesting technology is the most promise in terms of energy source availability, ease of implementation, and useful levels of output power. Each configuration has its own advantages and limitations, and in general, it is not possible for an energy harvester to perform well in all applications. For this reason, energy harvesters are normally designed for a specific application and a particular frequency range of operation. From state of the art, it became clear that some of these ambient energy sources are not always available in unlimited quantities. They fluctuate from time to time and from place to place depending on what time of day or season. They change from one season to another and from one region to another. For example traditional photovoltaics is not "always-on" power source, two major limits can be identified: the availability of light and the wavelengths that can be absorbed. Vibration (electromagnetic, electrostatic, piezoelectric, transducers) and triboelectric harvesters can generate power as soon as the aircraft start running. The RF is "always on ", however it has lowest energy density in an outdoor/indoor environment moreover, the power decreases with inverse square law $1/r^2$. Finally, thermal energy can generate power if there is a temperature gradient during the flight between for example electric engine and external air. On the NAV, temperature gradients may not occur straight away after take-off or there are few or no temperature gradients during the cruise. With an accurate knowledge of the environment, one could combine two or more energy harvesters to provide perpetual sources of electrical energy to Nano robot. Combining two or more sources increases the chance of having constant power supply at all times such that when one form is not available in sufficient quantity, the other will complement the temporary shortage. This technique is presented as hybrid energy harvesting techniques. Unfortunately, this technique is ideal in this context; in fact, it is impossible to add extra weight to Nano flight robots [26,27]. This author et al. have investigated the concepts and possibility of harvesting plasmonic energy in a mini UAV. Earth receives solar radiation only during the daylight hours; but emits mid-infrared (Mid- IR 7-14 μm) radiation during both the day and the night hours with a peak wavelength of about $10\,\mu m$ [8,9]. The proposed technique employs plasmonic Rectennas that absorb the incident IR radiation treating it as electromagnetic waves. Particular Nano Antennas (used as Nano generators) tuned in Mid-IR and integrated to rectifiers (Rectennas) can harvest IR energy from the sun night and day and convert it into electricity. Plasmonic Nano-Generator can operate round the clock, independently of weather conditions such as humidity and cloud cover and without restriction of orientation towards the sun.

3.2 Rectenna architecture and circuit model of IR antenna coupled to rectifying diode.

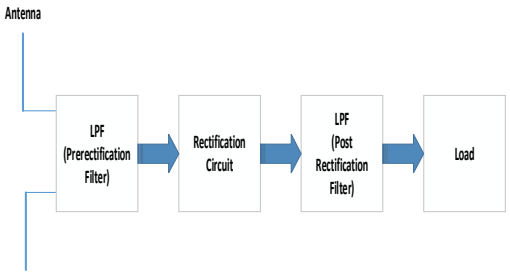

Figure 7: Rectenna equivalent circuit.

The sun emits shortwave radiation (visible light and near infrared) because it is extremely hot and has a lot of energy to give off. Once in the Earth's atmosphere, clouds and the surface absorb the solar energy. The ground heats up and re-emits energy as longwave radiation in the form of infrared rays (LWIR) [12] because Earth is cooler than the sun and has less energy available to give off. Typical rectenna block diagram is presented in Figure 7. The word "rectenna" is the result of joining "rectifying circuit" and "antenna". The rectenna is a passive element with a diode that can receive and rectify MID- IR power to DC, it can operate without any power source. The first block are the nanoantennas. They are small structures that capture the incident electromagnetic re-emitted from Earth' surface causing an AC current onto the antenna surface. For the nanoantenna is required to capture MID-IR radiation. For this purpose, a wide acceptance angle is essential. Nanoantennas, should be able to concentrate the incoming radiation, therefore a wideband antenna is favorited. The matching between the antenna and the rectifier is provided by low-pass filter [28]. Its aim is suppressing possible unwanted higher harmonics rejected by the nonlinear diode. These could come back to the nanoantenna resulting in power losses [29]. The diode is the most important device to achieve high-energy conversion efficiency. These types of rectifier should be coplanar and coupled to the nanoantenna. The requirements for an ultra-high speed diode used to obtain a DC signal are responsivity, small size, small turn on voltage and efficient performance at MID-IR frequency. Impedance matching between the rectenna system and the load is required to transfer the maximum power to load. This is possible when the load impedance is the conjugation of the rectenna impedance. Finally, the last block DC pass filter between diode and load provides a DC path to the load by separating the high-frequency components from the DC signal. The energy conversion efficiency of a rectenna structure essentially it depends on two elements, the nanoantenna and the

diode [29] which implies nanoantenna efficiency, impedance matching between nanoantenna and rectifying element and the coupling efficiency of the rectifier to the load. Therefore, the product of the efficiencies of each step determines the rectification efficiency (η) of a Rectenna as follows [11, 30, 31]:

$$\eta = \eta_a \eta_s \eta_c \eta_q \tag{12}$$

The antenna efficiency, which corresponds to the total power coupled by the antenna per unit of intercepted power, is represented by η_a. An antenna designed for IR harvesting operates as a receiving antenna that interacts with the incident EM wave. The incident wave induces current on the metal antenna surface, which constitutes the power coupled by the antenna. Figure 8 shows the equivalent circuit of the antenna coupled to rectifying diode. The receiving antenna, when operating at its resonant frequency, can be modeled by a voltage source, V_A, and an impedance in series, $Z_A = R_A + jX_A$. V_A is the open circuit voltage occurring at the end of the antenna when no load is connected and Z_A is the antenna impedance, where X_A is the antenna reactance and R_A is the antenna resistance which is a combination of the radiation resistance R_{rad} (radiated power by antenna), in series with the loss resistance R_{ohmic} (conductive and dielectric losses of antenna)[12].

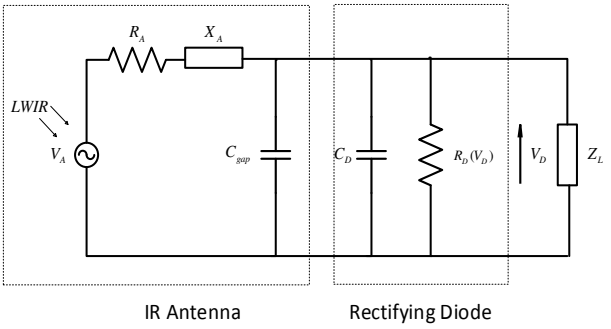

Figure 8: Circuit model of IR antenna coupled to rectifying diode.

Air-gap between two-arm antenna is modeled with the capacitance C_{gap}. The MIM tunnel diode is modeled with a voltage dependent resistor $(R_D(V))$ in parallel with a capacitor (C_D) and a resistor (r) in series for the conductive losses on the antenna arms. The cutoff frequency f_c, characterizing the frequency response of the diode, depends on both the diode resistance and capacitance as follows [12]:

$$f_c = \frac{1}{2\pi R_D C_D} \tag{13}$$

When resistance R_D depends on the fabrication process, the cutoff frequency can be tuned by adjusting the capacitance C_D. The diode capacitance is given by:

$$C_D = \frac{\varepsilon_r \varepsilon_0 A}{d} \tag{14}$$

where ε_r represents the relative permittivity of the insulator layer of the MIM diode, ε_0 is the permittivity of free space, A is the diode junction area (overlapping area), and d is the thickness of the insulator layer. The MIM diode cut-off frequency is determined by the time constant, $\tau_D = R_D C_D$ [12]. When the antenna is coupled to the diode, the cutoff frequency of the rectenna is rewritten as [12]:

$$f_c = \frac{R_A + R_D}{2\pi R_A R_D (C_{gap} + C_D)} \tag{15}$$

The total power provided by this voltage source is determined by the antenna efficiency η_a. The next efficiency component considers the losses that occur while the currents at the antenna surface flow onto the antenna node where the tunnel junction is formed. It is represented by η_s. This parameter strictly depends on the material conduction property at the operating frequency. The impedance matching between the antenna radiation resistance and the diode resistance forms a very crucial component of the total efficiency, represented by η_c (equation 16). The tunnel diode is characterized with a capacitive and a voltage dependent resistor in this circuit model. In order to achieve efficient coupling with the input power it is important to keep the diode resistance R_D value as close as possible to the antenna resistance R_A. Here the junction resistance value should be the value at the operating bias voltage, which is zero-bias $R_D(0)$ for IR harvesting applications and $R_D(V_{bias})$ for IR detecting case. $R_D(V_{bias})$ is always lower than $R_D(0)$ due to the nonlinear I-V characteristic of tunnel diodes. Lastly, η_q is the quantum efficiency derived in equation 17:

$$\eta_c = \frac{R_D}{R_D + R_A} \tag{16}$$

$$\eta_q = \frac{1}{2}\frac{\hbar\omega}{e} \cdot S \tag{17}$$

The rectenna's responsivity "S" measured in A/W, is the quantification of the diode's ability to rectify a Terahertz signal. It is defined as: $S = \frac{I^{''}(V_{bias})}{I^{'}(V_{bias})}$, $I^{'}(V_{bias})$ and $I^{''}(V_{bias})$ are the first and the second derivative of the electric current passing through the diode at a certain bias voltage. The incident electric field E_{rms} can be related to the Poynting vector using the vacuum impedance Z_0.

$$Z_0 = \sqrt{\frac{\mu_0}{\varepsilon_0}} = 377\Omega \tag{18}$$

The incident power intensity or Poynting vector (ξ) is the time averaged power per unit area A of the incident radiation:

$$\xi = \frac{P_{inc}}{A} = \frac{E_{rms}^2}{Z_0} = \frac{E_p^2}{2 \cdot Z_0} \; [W/m^2] \tag{19}$$

The amplitude of the coupled potential across the antenna arms V_A is related to the incident electric field (E_p) and the effective antenna length l_{eff} as in Equation 20. The effective antenna length (l_{eff}) is a function of the incident wave direction and the antenna length L_{ant} as formulated in Equation 21. When the beam is incident perpendicularly $\theta = 90^{\circ}$, l_{eff} can be approximated as the antenna physical length L_{ant}:

$$V_A = l_{eff} \cdot E_p \tag{20}$$

$$l_{eff} = L_{ant} \sin(\theta) \tag{21}$$

Here an important parameter called antenna aperture efficiency or antenna fill factor comes into play. Antenna fill factor f can be defined as in Equation 22. It is a dimensionless parameter and is equivalent to product between antenna coupling efficiency η_a and the losses η_s by material. Conceptually, it describes how well the antenna can couple the incident radiation:

$$f = \frac{A_{eff}}{A} = \frac{L_{ant}^2}{A} = \eta_a \eta_S \tag{22}$$

A_{eff} is the effective area of the antenna defined as :

$$A_{eff} = \frac{\lambda^2 G}{4\pi} \tag{23}$$

where G is the antenna gain and λ is the free-space wavelength.

Thus, the coupled voltage V_A can be expressed in terms of the incident power as:

$$V_A = \sqrt{\frac{P_{inc} \cdot 2Z_0 \cdot L_{ant}^2}{A}} = \sqrt{P_{inc} \cdot 2Z_0 \cdot f} \tag{24}$$

Therefore, the induced voltage in the equivalent circuit is proportional to the square root of the radiation resistance and the maximum effective aperture. When the AC electric field excites surface electrons, their motion on the antenna surface induces an electric field and a fraction of the coupled power is re-radiated. This loss in the re-radiated power is represented by a virtual resistance called "antenna radiation resistance R_A " and it is determined by the geometry of the antenna. The antenna coupling efficiency can also be formulated by circuit representation where the total radiation power is shared between the vacuum impedance Z_0 and antenna radiation resistance R_A as in Equation 25:

$$f = \frac{R_A}{R_A + Z_0} \tag{25}$$

Once the antenna potential is defined in terms of the incident radiation, the impedance matching efficiency η_c should be used to define the power across the diode as in Equation 26:

$$P_D = \frac{|V_A|^2 R_D}{2[(R_{rad} + R_{ohmic} + R_D)^2 + (X_A + X_D)^2]} \tag{26}$$

and the power dissipated in the antenna is given by:

$$P_{ohmic} = \frac{|V_A|^2 R_{ohmic}}{2[(R_{rad} + R_{ohmic} + R_D)^2 + (X_D + X_A)^2]} \tag{27}$$

$$P_{rad} = \frac{|V_A|^2 R_{rad}}{2[(R_{rad} + R_{ohmic} + R_D)^2 + (X_A + X_D)^2]} \tag{28}$$

Note that P_{rad} is the scattered (or re-radiated) power by antenna. This scattered power does not exist as a separate measurable independent quantity of real power that enters into any statement of power conservation.

However, the scattered wave determines the amount of captured power by the antenna through interference with the incident wave. The first component of total efficiency is defined as power transfer efficiency (η_t). This term determines the fraction of the incident power that can reach the diode from the antenna section. It can be derived as in Equation 29 using Equations 26 and 24:

$$\eta_t = \eta_a \cdot \eta_s \cdot \eta_c = \frac{P_D}{P_{inc}} = \frac{2 \cdot f \cdot Z_0 \cdot R_D}{(R_A + R_D)^2 + (X_A + X_D)^2} \quad (29)$$

When $R_D >> R_A : \eta_t = \frac{2 \cdot f \cdot Z_0}{R_D}$.

The total efficiency, which is the ratio of the detected DC power and the incident radiation power, can be defined as in Equation 30:

$$\eta = \eta_t \cdot \eta_q = \frac{2 \cdot f \cdot Z_0 \cdot R_D}{(R_A + R_D)^2 + (X_A + X_D)^2} \cdot \frac{1}{2} \frac{\hbar \omega}{e} \cdot S \quad (30)$$

3.3 Nano Antennas tuned in MID-IR

There are two important aspects of the antenna design: geometry and material. The need of a broadband antenna is mandatory. An antenna pattern that can accommodate wide polarization angle span of the incident wave is necessary to increase the total coupled power. Ideally, the material used in the construction of the Nano-Antenna should exhibit no losses during the collection of electromagnetic radiation. However, this is hardly achievable due to the finite conductivity of metals at THz frequencies [31]. In this paper, three broadband antennas tuned to the Mid-IR region of the spectrum are analyzed, as potential systems for harvesting thermal radiation.

3.3.1 Log Periodic Antenna (LPA)

Rumsey's principle suggests that the impedance and pattern properties of an antenna will be frequency independent (will have a constant impedance at all frequencies) if the antenna shape is specified only in terms of angles. To satisfy the equal-angle requirement, the antenna configuration needs to be infinite in principle, but is usually truncated in size in practice [32]. Rumsey's principle has been verified in spiral antennas, and some log periodic antennas. DuHamel and Isbell [32] first introduced the Log-periodic antenna. It is designed to work among a wide range of frequencies. Larger bandwidth is obtained by means of the insertion of a set of teeth, whose lengths are suitably chosen to be resonant in some frequencies inside the desired bandwidth. Gonzàlez et al. [33] designed a log periodic antenna for IR application with a scale factor of $\tau = 2$, coupled to a niobium microbolometer. The materials and fabrication of this antenna is reported on [33]. If $\beta_1 + \beta_2 = 90^\circ$ the antenna becomes self-complementary in which case it will have a constant impedance of 189 Ω at all frequencies [33]. The log-periodic antenna was designed to have a frequency coverage of 18–70 THz which corresponds to a wavelength coverage of 4-16 μ m. For IR application the wavelength measured were at 10.6 μm and the radiation efficiency for log periodic IR antennas was 46%.

3.3.2 Spiral Nano-antenna

Spiral Nano Antenna is a planar structure frequency independent [32]. Two types of Nano antennas are presented: Archimedean spiral geometries and square spiral geometries. Both good resonators they can be polarized with linearly and circularly waves. The electric field is concentrated in the gap between two metallic arms. Increasing the number of arms increases the electric field and its aperture area. The square spiral Nano-Antenna proposed by Sabaawi et al [34] has 6 arms with an arm width of 50 nm, a gap of 50 nm, and overall dimensions of $1.25\mu m \cdot 1.25\mu m$. At resonance of 13 μm the electric field E into the gap is $6.2 \cdot 10^{-3} V / \mu m$. Sabaawi et al [35] designed also a square spiral Nano-Antenna with dimension of $750 \cdot 750$ nm , and a gap size of 30 nm. The max electric field E captured into the gap, at the resonance of about 13μm is $0.575 \cdot 10^{-3}$ V /μm . The Archimedean spiral Nano-Antenna consists of two identical arms with a shift of 180° with respect to each other. Ahmed M. A. Sabaawi et al [34] showed the configuration of the Archimedean-Spiral Nano-Antennas. The configuration is designed to resonate around 13μm. The electric field E in the gap of the single Archimedean Spiral Nano-Antennas is $5.8 \cdot 10^{-3} \mu$V / m . With the MIM diode, embedded in the feeding gap the efficiency has a value about 10^{-12} for spiral antennas. With Esaki diode, a device that consists of an insulating layer between two thin electrodes and it based on the tunnel effect is obtained an efficiency about 10^{-9} [29]. Sabaawi et al [34] show also a Nano-array made with two Archimedean spiral antennas with one common gap. The electric field presented has been of $1.84 \cdot 10^{-3}$ $V / \mu m$. A Nano-array made with four Archimedean spiral antennas with one common gap presets an electric field of $6.58 \cdot 10^{-3}$ $V / \mu m$. Although is not easy building an array of these antennas some advantage are: one only rectifier embedded in the feeding gap, improvement of equivalent area and largest value of Electric field compared to single antenna.

3.3.3. *Bowtie Nano-antenna*

The Bow-Tie Nano-Antenna consists of two triangular flat metal plates with a gap between the apexes of the triangles. This structure produces a stronger electric field in the gap where a rectifier can be embedded. The main advantages of bowtie antennas are simple design, broadband impedance and only defined by the bow

angle θ. This configuration gives the designer the freedom to vary several antenna parameters. Gap size, apex angle and antenna dimensions could be tuned in order to increase the captured electric field in the gap [32]. This nanoantenna allows building an array by coupling each element in one configuration. The total electric field at feeding point will be the sum of electric field of each single bow tie antenna. To achieve an output DC signal, the bowtie nanoantenna is coupled with an MIM (Metal Insulator Metal) [36]. Gadalla et al [37] proponed the structure with Au/Al2O3/Pt. MIM diode is overlapped with antenna arms, the utilization of different electrodes produces a higher value of tunneling current. The tunneling current can be improve increasing the work function difference between the two different metal and reducing the contact area of the tunnelling junction; as a consequence, it is obtained a better impedance matching between antenna and diode. The Au/TiOx/Ti MIM diode is chosen because gold and titanium are characterized by a large difference in the work function and so a strong rectifying effect is achieved [29,38,39]. A. Haque et al [40] present the geometric effect (slot) on the performance of the circular edge bow-tie nano antenna in the IR frequency range. The proposed antenna is designed to receive induced electric field at the central gap. The electric field is then transferred via a feeding line and converted into electric current to supply the load. The materials and fabrication of this antenna are reported in [40]. Antenna with double slot provides better electric field compared to the antennas without slot or with single slot. Resonance frequency also changes with the change of the number of slots.

4.0 Rectifying Element

The diode represent the essential component of rectenna. The rectenna is limited by the cut-off frequency (fc) of the diode, fc changes with the type of rectifier used due to the physical nature of the diode. However, for MID-IR application a low RC time constant is mandatory. Two types of diodes are presented. Schottky barrier diodes where electron moves across the barrier by a thermal activation and MIM (metal-insulator-metal) and MIIM (metal-insulator-insulator-metal) diodes where electron moves across the barrier for tunneling effect [41,42]. Schottky barrier diodes are theoretically limited to frequencies of a few THz, due to relatively higher resistance of semiconductors compared to metals. MIM/MIIM diodes have fast electron switching speeds, of the order of 10 fs [37], and use metal electrodes, thus providing a low resistance. Therefore, they can be used at higher frequencies than Schottky barrier diodes and are shown to be operational at up to 150 THz [41, 42,43,44]. To improve the rectenna efficiency, the diode must satisfied several parameters [41]:

$$f_{asym}(V) = \left| \frac{I_F(V)}{I_R(V)} \right|; \text{Asymmetry>1} \tag{31}$$

$$f_{NL}(V) = \frac{\frac{dI}{dV}(V)}{\frac{I(V)}{V}}; \text{Nonlinearity>3} \tag{32}$$

$$f_{RES}(V) = \frac{\frac{d^2I}{d^2V}(V)}{\frac{dI}{dV}(V)}; \text{Responsivity> } 7V^{-1} \tag{33}$$

The asymmetry FOM (Figure of Merit), defined in Equation 31, is the absolute ratio of forward to reverse current at a bias, a value of 1 indicating full symmetry and hence no rectification. The non-linearity FOM, as defined by Equation 32, is the ratio of the differential conductance to the conductance and is a measure of the deviation from a linear resistor. Finally, the responsivity FOM defined in Equation 33 is the ratio of the second derivative of the I-V curve and the differential conductance and is a measure of the rectified signal as a function of input power. The rectification process will be more efficient if the diode will exceeds the values in equations 31,32,33. Moreover, the MIM diode must be very fast to IR regime therefore 1) the insulator layer should be on the order of a few nanometers, by doing so, it is possible to allow sufficiently large electrical current and to ensure the tunneling effect 2) diode capacitance must be small, as consequence, the device area must be small below 1 μm^2 (equation 14). To respect the MID-IR regime (30 THz) however, the diode must have also a low resistance close to the nanoantenna resistance (to provide a good impedance matching antenna-diode and an efficient power transfer), it must pass a large current at low voltage, as consequence should have a large area. Currently this tread-off restricts the use of MIM diode [29]. In this review are presented two types of diodes: low voltage tunnel diodes and ultralow-voltage diodes [29]. An example of low voltage tunnel diode in MID-IR rectennas is the metal-insulator- metal (MIM) diode. The performance of MIM and MIIM diodes as infrared detectors are reported in the literature. For MIM Donchev [41] shows a Nb/Nb2O5/Ag device, the results are 35.6 asymmetry, 4.0 nonlinearity and 7.9 V^{-1} responsivity. Yaksh Rawal et al [45] show a new type of MIM diode Ti/TiO2/Al (21287 μm^2 area) with 9nm-thickness dielectric layer, 18 sensitivity $\left(V^{-1}\right)$ and 6.5 asymmetry. The Ni/NiO/Ni system is widely used for detection and mixing up to 30 THz infrared radiation due to its significantly low resistance-area product of 1Ω (μm^2) [41, 46,47,48, 49, 50], which indicates the potential for a low RC constant. However due to a lack of asymmetry, the second Ni electrode must be replaced with a metal of different work function in order to achieve rectification. This has been investigated by

Hoofring et al [51], Krishnan et al [52, 53] and Esfandiari et al [54] with Au, Cr and Pt contacts respectively, all displaying good asymmetrical I-V response. Other structures of dissimilar materials which have shown promising results are Al/Al2O3/Ni [55,56], Nb/Nb2O5/Pt [57, 58, 59], ZrCuAlNi/Al2O3/Al [60] and also Nb/Nb2O5/Ag [61]. More tested metal-insulator combinations are listed in [57]. The highest FOMs were observed for Nb/Nb2O5/Pt, which displayed 1500 asymmetry, 4 nonlinearity and 20 V^{-1} responsivity meeting the criteria outlined in Equations 31, 32 and 33. An MIM diode can have asymmetric *I–V* if different metals are used on the two sides of the insulator with great work function difference between them, giving unequal barrier heights. High barrier asymmetric diodes provide a large responsivity. However, keeping the diode resistance low requires low barrier heights on both sides, which limits the asymmetry. To achieve a high responsivity, requiring substantial nonlinearity while maintaining low resistance, one can resort to a multi-insulator tunnel barrier (MIIM) [62,63]. With MIIM asymmetry can be achieved even with similar metal electrodes, as long as the electron affinity of both insulators is different. The performance of MIM and MIIM diodes as infrared detectors was compared by Hegyi et al [64]. It was shown that the MIIM diode has 10 times higher responsivity than a derivative MIM diode. This was experimentally shown by Maraghechi et al [65] who recorded up to 10 times better nonlinearity for a Cr/Al2O3/HfO2/Cr diode compared to Cr/Al2O3/Cr and Cr/HfO2/Cr diodes. A more applicable example is by Grover & Moddel [66], who compared their W/Nb2O5/Ta2O5/W structure to an MIM Diode with equivalent barriers as that of a W/Nb2O5 on one side and a W/Ta2O5 on the other side, again clearly showing improved response from the MIIM device. Finally, ultralow-voltage diodes we call geometric diode is presented. A geometric diode consists of a thin film with an asymmetric structure no greater in size than the MFPL (mean-free path length) in which charge carriers move more easily to the left than to the right. This planar structure avoids the capacitance/resistance tradeoff because it is not a sandwich structure. Made out of a conductive material, it can have both low resistance and ultra-low capacitance [67].

5.0 Conclusion Remarks

The progress and challenges of Rectennas to harvest energy from Earth long-wave infrared emission have been reviewed. However the accurate design of the antenna, and in particular rectifiers, remains a key topic. The use of broadband antennas for collecting MID-IR infrared Earth's energy has a big potential advantage. Even though the tunneling process is femtosecond fast, MIM tunnel diodes are frequency limited due to their large RC time constant. Searching for a diode suitable for solar rectification, in addition to high speed and responsivity, the goal must be a device that has a combination of lower resistance and lower capacitance than the existing MIM diodes. Moreover, further research activities have to be fulfilled to identify the suitable materials and technology for the design and fabrication of efficient THz rectifiers.

Reference

[1] Chin C K, Extending the Endurance, Mission and Capabilities of Most UAVs using Advanced Flexible/Ridged Solar Cells and New High Power Density Batteries Technology, Master of science in Electrical Engineering, Monterey California, March 2011

[2] Petricca L, Ohlckers P, and Grinde C 2011 Micro- and Nano-Air Vehicles: State of the Art, International Journal of Aerospace Engineering, Hindawi, Volume 2011, pp.1- 17

[3] Prox Dynamics Personal Reconnaissance System PD-100 Black Hornet, 2014, pp.1-6

[4] Petricca L, Micro and Nano Technologies for Unmanned Nano Air Vehicles (NAVs), PhD Thesis, Buskerud and Vestfold University College, 2014

[5] Dudek M, Tomczyk P, Wygonik P, Korkosz M , Bogusz P and Lis B 2013 Hybrid Fuel Cell – Battery System as a Main Power Unit for Small Unmanned Aerial Vehicles (UAV), International Journal of Electrochemical Science Vol.8, pp.1-22

[6] Wang Z L, Zhu G, Yang Ya, Wang S, and Pan C, 2012, Progress in nanogenerators for portable electronics, Elsevier, Volume 15, Number 12, pp. 532–543

[7] Montagnier O and Bovet L 2010, Optimization of a Solar-Powered high altitude long endurance UAV, *Proc. Int. Conf. on Aeronautical Sciences*(France), pp.1-10

[8] Rapinett A and Zephyr: A High Altitude Long Endurance Unmanned Air Vehicle, Master thesis in Physics, University of Surrey, 2009

[9] http://www.phy6.org/stargaze/Isun1lite.htm

[10] http://www.ces.fau.edu/nasa/module-2/energy-budget.php

[11] http://www.photonics.com/Article.aspx?AID=45403

[12] Mescia L and Massaro A, 2014, New Trends in Energy Harvesting from Earth Long-Wave Infrared Emission, Hindawi, Volume 2014, pp-1-11

[13] Demir KA, Cicibas H and Arica N, 2015, Unmanned Aerial Vehicle Domain: Areas of Research, Defence Science Journal, Vol. 65, No. 4, pp. 319-329

[14] Biblioscholar, 2007, Nano Air Vehicles a Technology Forecast, pp.1-43

[15] Waharte S and Trigoni N 2010 Supporting Search and Rescue Operations with UAVs, *Proc. Int. Conf. on Robots and Security*, *Oxford,* pp.1-6

[16] https://www.microdrones.com/en/applications/areas-of-application/search-and-rescue/

[17] http://wiki.mikrokopter.de/MK3538#Thrust_over_current

[18] http://www.rcdronegood.com/quadcopter-battery-calculator-flight-times/

[19] https://oscarliang.com/how-to-choose-battery-for-quadcopter-multicopter/

[20] http://wiki.mikrokopter.de/en/FlightTime

[21] Theilmann CA Integrating Autonomous Drones into the National Aerospace System, Master of Science, University of Pennsylvania, 2015

[22] Penella-López MT and Gasulla-Forner M 2011 *Powering Autonomous Sensors*, Springer

[23] Penella MT and M. Gasulla M A 2007 Review of Commercial Energy Harvesters for Autonomous Sensors, *Proc. Int. Conf on Instrumentation and Measurement Technology*, Warsaw, Poland, IEEE, pp. 1-5

[24] Rahimi M, Shah H and Sukhatme GS 2003 Studying the Feasibility of Energy Harvesting in a Mobile Sensor Network , *Proc. Int. Conf on Robotics & Automation* (Taipei Taiwan), IEEE pp.14-19

[25] Kansal A, Hsu J, Zahedi S and Srivastava MB 2007 Power Management in Energy Harvesting Sensor Networks, *Proc. Int. Conf on Embedded Computing Systems*, Vol. 6, No. 4, Article 32,NY USA, pp.1-38

[26] LU Y, Savvaris A, Tsourdos A, Bevilacqua M 2016 Vibration Energy Harvesters for Wireless Sensor Networks for Aircraft Health Monitoring , *Proc. Int. Conf on Metrology for Aerospace (MetroAeroSpace)*, Florence, Italy, IEEE, pp. 1-8

[27] Álvarez-Carulla A, Colomer-Farrarons J, López-Sánchez J, Miribel-Català P 2016 Piezoelectric Harvester-Based Structural Health Monitoring that Uses a Self-Powered Adaptive Circuit , *Proc. Int. Conf on* Metrology for Aerospace (MetroAeroSpace), Florence, Italy, IEEE, pp.1-5

[28] Gadalla MN 2013 Nano Antenna Integrated Diode (Rectenna) For Infrared Energy Harvesting, Master of Science, King Abdullah University of Saudi Arabia

[29] C. Di Garbo, P. Livreri and G. Vitale, 2016, Review of Infrared Nanoantennas for Energy Harvesting, *Proc. Int. Conf. on* Modern Electrical Power Engineering (las Palmas de Gran Canaria 6 - 8 of July), pp.1-7

[30] Moddel G and Grover S 2013 Rectenna Solar Cells, Springer

[31] Yesilkoy F 2012 IR Detection and Energy Harvesting Using Antenna Coupled MIM Tunnel Diodes, PhD Dissertation, University of Maryland

[32] DuHamel R.H and Isbell D.E. 1966 Broadband Logarithmically Periodic Antenna Structure, *Proc. Int. Conf on Antennas & Propagation*, (NY, USA) pp. 119 - 128

[33]Gonzalez FJ, Boreman GD 2004 Comparison of dipole, bowtie, spiral and log-periodic IR antennas, Elsevier, volume 46, pp.1-12

[34] Sabaawi A M A , Tsimenidis CC and Sharif BS 2011 Infra-red nano-antennas for Solar Energy Collection, *Proc. Int. Conf on Antennas & Propagation*, (Loughborough, UK), pp.1-4

[35] Sabaawi AMA, Tsimenidis CC, and Sharif BS 2012 Infra-red Spiral Nano-antennas, *Proc. Int. Conf on Antennas & Propagation, (*Loughborough, UK), pp.1-4

[36] Grover S and Moddel G 2011 Applicability of Metal/Insulator/Metal (MIM) Diodes to Solar Rectennas , IEEE, Vol. 1, No.1, pp.1-6

[37] Gadalla, M. N., Abdel-Rahman, M. & Shamim, A. Design, optimization and fabrication of a 28.3 thz nano-rectenna for infrared detection and rectification. Scientific Reports 4, 4270 (2014).

[38] K. Wang, H. Hu, S. Lu, L. Guo and T. He "Design of a sector bowtie nano-rectenna for optical power and infrared detection" Frontiers of Physics 10, 5, pp. 1-12, 2015.

[39] M Aldrigo, D Masotti, A Costanzo, V Rizzoli, 2013, Numerical analysis of an innovative energy-harvesting system in the infrared region, *Proc. Int. Conf. on* Wireless Power Transfer (WPT), IEEE pp. 1-5

[40] A Haque, A W Reza, N Kumar, H Ramiah, 2015, Slotting Effect in Designing Circular Edge Bow-Tie Nano Antenna for Energy Harvesting, *Proc. Int. Conf. on* Open Systems (ICOS), Melaka, Malaysia, pp. 1-5

[41] Donchev E 2015 Thin-Film Diode Structures for Advanced Energy Applications, PhD thesis, Imperial College London

[42] G Moddel, Z Zhu and S Grover, 2011, Solar power conversion using diodes coupled to antennas, Spie, pp.1-3

[43] Berland, B. Photovoltaic technologies beyond the horizon: Optical rectenna solar cell. Subcontractor Report, National Renewable Energy Laboratory (2002). URL http:// www.nrel.gov/docs/fy03osti/33263.pdf.

[44] Jennings, D., Petersen, F. R. & Evenson, K. Extension of absolute frequency measurements to 148 thz: Frequencies of the 2.0 and 3.5 μm xe laser. Applied Physics Letters 26, 510-511 (1975).

[45] Rawal Y, Ganguly S, and Baghini MS 2012 Fabrication and Characterization of New Ti-TiO2-Al and Ti-TiO2-Pt Tunnel Diodes, Hindawi, Vol. 2012, pp.1-6

[46] Abdel-Rahman, M. R., Gonzalez, F. J. & Boreman, G. Antenna-coupled metal-oxide-metal diodes for dual-band detection at 92.5 ghz and 28 thz. Electronics Letters 40, 116-118 (2004).

[47]Fumeaux, C., Herrmann, W., Kneubuhl, F. K. & Rothuizen, H. Nanometer thin-film diodes for detection and mixing of 30 (THz) radiation. Infrared Physics & Technology 39, 123-183 (1998).

[48] Abdel-Rahman, M. R., Gonzalez, F. J. & Boreman, G. Antenna-coupled metal-oxide-metal diodes for dual-band detection at 92.5 ghz and 28 thz. Electronics Letters 40, 116-118 (2004).

[49] Fumeaux, C., Herrmann, W., Kneubuhl, F. K. & Rothuizen, H. Nanometer thin-film diodes for detection and mixing of 30 THz radiation. Infrared Physics & Technology 39, 123-183 (1998).

[50] Hobbs, P. C. D., Laibowitz, R. B. & Libsch, F. R. Ni-nio-ni tunnel junctions for terahertz and infrared detection. Appl. Opt. 44, 6813-6822 (2005).

[51] Hoofring, A. B., Kapoor, V. J. & Krawczonek, W. Submicron nickel-oxide-gold tunnel diode detectors for rectennas. Journal of Applied Physics 66, 430-437 (1989).

[52] Krishnan, S., La Rosa, H., Stefanakos, E., Bhansal, S. & Buckle, K. Design and development of batch fabric able metal insulator metal diode and microstrip slot antenna as rectenna elements. Sensors and Actuators A: Physical 142, 40-47 (2008).

[53] Krishnan, S., Stefanakos, E. & Bhansali, S. Effects of dielectric thickness and contact area on current voltage characteristics of thin film metal insulator metal diodes. Thin Solid Films 516, 2244{2250 (2008).

[54] Esfandiari, P. et al. Tunable antenna-coupled metal-oxide-metal (mom) uncooled IR detector (invited paper). vol. 5783, 470-482.

[55] Gustafson, T. K., Schmidt, R. V. & Perucca, J. R. Optical detection in thin- film metal-oxide- metal diodes. Applied Physics Letters 24, 620-622 (1974).

[56] Dickinson, R. M. & Brown, W. C. Radiated microwave power transmission system efficiency measurements. Tech. Rep. Tech. Memo 33-727, Ames R.C. Rsch. Review, NASA, California Inst. Technol. Pasadena, CA, USA (1975).

[57] Periasamy, P. et al. Fabrication and characterization of mim diodes based on nb/nb2o5 via a rapid screening technique. Advanced Materials 23, 3080-3085 (2011).

[58] Periasamy, P. et al. Metal insulator metal diodes: Role of the insulator layer on the rectification performance. Advanced Materials 25, 1301-1308 (2013).

[59] Periasamy, P. et al. A novel way to characterize metal-insulator-metal devices via nanoindentation. In Photovoltaic Specialists Conference (PVSC), 2011 37th IEEE, 001754-001757 (2011).

[60] Cowell, E. W. et al. Advancing mim electronics: Amorphous metal electrodes. Advanced Materials 23, 74-78 (2011).

[61] Grossman, E. N., Harvey, T. E. & Reintsema, C. D. Controlled barrier modification in nb/nbox/ag metal insulator metal tunnel diodes. Journal of Applied Physics 91, 10134-10139 (2002).

[62] Hagerty, J., Helmbrecht, F., McCalpin, W., Zane, R. & Popovic, Z. Recycling ambient microwave energy with broadband rectenna arrays. Microwave Theory and Techniques, IEEE Transactions on 52, 1014-1024 (2004).

[63] Bailey, R. L. A proposed new concept for a solar-energy converter. Journal of Engineering for Power 94, 73-77 (1972).

[64] Hegyi, B., Csurgay, A. & Porod, W. Investigation of the nonlinearity properties of the dc i-v characteristics of metal-insulator-metal (mim) tunnel diodes with double-layer insulators. Journal of Computational Electronics 6, 159-162 (2007).

[65] Maraghechi, P., Foroughi-Abari, A., Cadien, K. & Elezzabi, A. Y. Enhanced rectifying response from metal-insulator-insulator-metal junctions. Applied Physics Letters 99, 253503 (2011).

[66] Grover, S. & Moddel, G. Engineering the current voltage characteristics of metal insulator metal diodes using double-insulator tunnel barriers. Solid-State Electronics 67, 94-99 (2012).

[67] G Moddel, Z Zhu, and S Grover, 2011, Solar power conversion using diodes coupled to antennas, Spie, pp.1-3